Chemical Science

RSC Publishing

EDGE ARTICLE

View Article Online
View Journal | View Issue

Cite this: *Chem. Sci.*, 2013, 4, 509

Surface-enhanced Raman scattering (SERS) from Au:Ag bimetallic nanoparticles: the effect of the molecular probe†

Meikun Fan,[ab] Feng-Ju Lai,[c] Hung-Lung Chou,[c] Wan-Ting Lu,[c] Bing-Joe Hwang*[cd] and Alexandre G. Brolo*[b]

Surface-enhanced Raman scattering (SERS) from molecular probes adsorbed on Au:Ag bimetallic nanoparticles with various compositions was investigated. Au:Ag bimetallic nanoparticles (NPs), with the diameters between 3–5 nm, were prepared and characterized by HRTEM and UV-Vis absorption. Their SERS properties were examined by using four different probe molecules, and compared with NPs made of pure Au or Ag. It is found that the SERS property of the alloy NPs is not only dependent on the Au:Ag ratio of the bimetallic NPs, but also on the chemical nature of the SERS probe. For the two positively charged SERS probes, oxazine 720 (Oxa) and Nile Blue A (NBA), the alloy NPs with higher Au content provided the largest SERS signal. However, for the probes 4-hydroxythiophenol (HTP) and thiophenol (TP), the best SERS performance was obtained for the highest Ag ratio. DFT calculations indicated a charge-transfer between Au and Ag atoms in the alloys, creating positively charged domains rich in Ag atom, and negatively charge regions dominated by Au atoms. It is proposed that the probe-specific enhancement is related to the selective binding of probe molecules to the partially charged surface domains in the alloys. Our results suggest that SERS substrate optimizations based on bimetallic nanoparticles should consider the nature of the probes and the electronic-induced effects from the alloys.

Received 6th August 2012
Accepted 29th October 2012

DOI: 10.1039/c2sc21191b

www.rsc.org/chemicalscience

Introduction

Surface-enhanced Raman scattering (SERS) was first reported in 1970's,[1] and rapidly became a powerful analytical method for applications in fundamental and applied research.[2–6] One of the most active research fields in SERS is related to the quest for new substrates with improved enhancement efficiency and reproducibility. These efforts include several approaches, such as the development of new nanomaterials by top-down methods[2,7] and the self-assembly of nanoparticles in planar platforms.[8,9] Nanoparticles (NPs) of different sizes and shapes,[2,7] including periodical metallic structures[10,11] and multi-composition metallic materials,[12–15] have been explored in the search for optimized SERS substrates. It is important to emphasize that, since SERS is a resonance phenomenon, the optimal performance is defined for particular excitation conditions.[6]

One of the parameters explored in the pursuit for optimized SERS substrates is the composition of the nanomaterial. For instance, Au and Ag (the two most used plasmonic metals) can be combined in bimetallic NPs with novel optical properties.[16] In fact, Au:Ag bimetallic core–shell, as well as alloy NPs at different sizes and shapes, have attracted tremendous attention from the SERS community.[12–14,17–27] There are a few reasons to explore bimetallic nanostructures for SERS. It is widely accepted that Ag is a more effective plasmonic material than Au. However, Au provides advantages in terms of chemical stability. Bimetallic Au:Ag materials have the potential to combine the best of both metals in terms of chemical and plasmonic properties. Actually, previous reports show that Au:Ag NPs present higher SERS activity than the NPs made from either pure gold or silver.[12,14,19–22] The explanations for these experimental results included a pin-hole theory[28] and the effect of adsorbate-induced aggregation[20] favored at certain Au:Ag ratios. The pin hole explanation[28] states that the local electromagnetic field can increase by a factor of ~4 within pin holes in relative large-sized core–shell NPs (~40 nm or larger), leading to a better SERS efficiency relative to the pure metals. The adsorbate-induced aggregation applies to core–shell NPs suspended in a liquid phase.[20]

[a]*Chengdu Green Energy and Green Manufacturing R&D Centre, Chengdu, 610207, China*

[b]*Department of Chemistry, University of Victoria, PO Box 3055, Victoria, BC V8W 3V6, Canada. E-mail: agbrolo@uvic.ca*

[c]*Nanoelectrochemistry Laboratory, Department of Chemical Engineering, National Taiwan University of Science and Technology, Taipei 106, Taiwan. E-mail: bjh@mail.ntust.edu.tw*

[d]*National Synchrotron Radiation Research Center, Hsinchu 30076, Taiwan*

† Electronic supplementary information (ESI) available. See DOI: 10.1039/c2sc21191b

In this work, we explored the SERS properties of Au:Ag alloy NPs at different ratios. Four different SERS probes (molecules that yield SERS) were investigated. We showed that, in general, the SERS enhancement found from Au:Ag alloy NPs was larger than from pure Au or Ag. This behavior is in agreement with the literature.[12,21,25] However, we also report that the optimal condition (alloy composition) for SERS was dependent of the chemical nature of the probe. This is a very interesting observation that needs to be taken into consideration for the further development of SERS substrates from bimetallic metal alloys. DFT calculations were performed, and these surprising results were explained considering the electronic environment of the metals in the alloys.

Experimental section

Synthesis of Au:Ag bimetallic NPs

Tetrachloroaurate acid ($HAuCl_4 \cdot 3H_2O$, 99.90%), silver nitrate ($AgNO_3$), and ethylene glycol (EG, $C_2H_6O_2$, 99%) were purchased from ACROS. All the chemicals were used without any further purification. Au_xAg_{10-x} nanoparticles with various ratios were prepared by the EG method. In this case, the EG function as both reduction agent and solvent. Poly(*N*-vinylpyrrolidone) (PVP – MM $\sim$ 58 000 g mol^{-1}) was used to cap the metal and avoid aggregation. The metal : PVP molar ratio in the reaction system was 0.01. The PVP was dispersed in 80 ml of EG and the appropriate amount (proper molar ratio to produce the desired composition of the alloy) of $HAuCl_4 \cdot 3H_2O$ and $AgNO_3$ was added to the solution. The pH of the reaction mixture was brought to 10 by the drop-wise addition of saturated sodium hydroxide solution. The whole reaction mixture was then refluxed at 120 °C for 1 h. PVP is a well-known steric stabilization agent for both Au and Ag nanoparticles. This work shows that it can also stabilizes well Au:Ag alloy NPs at any composition.

Characterization methods

UV-Vis absorption spectra were collected on an Analytik Jena SPECORD S 100 spectrometer using quartz cuvettes. High-resolution transmission electron microscopy (HRTEM) images were obtained with a FEI-TEM 2000 instrument operating at an acceleration voltage of up to 200 kV. Samples for HRTEM measurements were prepared by using a sonicator to disperse the NPs in ethanol and placing a drop of the colloidal dispersion on a Cu grid, followed by drying in the oven.

SERS measurements

The NPs were drop-casted onto glass slides and dried using a hotplate, followed by rinsing with MeOH. 10 μL methanolic solution of the probe molecules were drop coated onto the NPs aggregates. After the solvent evaporated, the substrates were further rinsed with MeOH a few times before measurement. Four probe molecules (oxazine 720 (Oxa, 10 μM), nile blue A (NBA, 10 μM), thiophenol (TP, 1 mM), and 4-hydroxythiophenol (HTP, 1 mM)) were all from sigma and were used without further purification. The probe molecules represent two groups of two species with similar structure (the chemical structures are provided as ESI, Fig. S2†). The SERS spectra from the different probes adsorbed on the alloys of variable compositions were recorded using a Renishaw in-via spectrometer equipped with a microscope and a 50× objective (numerical aperture of 0.75). The spectral bandwidth of the system was 2 cm^{-1}. Typical spectral collection parameters for 632.8 nm were 2 s acquisition time and 10 accumulations; and for 785 nm, the exposure time was 1 s and the SERS signal was accumulated 10 times as well.

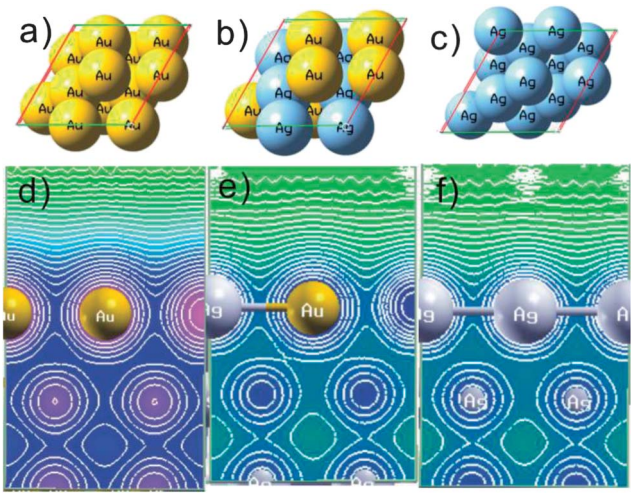

Fig. 1 Model used in the DFT calculations (a) top-view of Au(111), and (b) top-view of AuAg(111), and (c) top-view of Ag(111). (d) the contour plot of Au(111) and (e) AuAg(111), and (f) Ag(111) slabs.

DFT calculations

DFT simulations were performed using Au(111), AuAg(111), and Ag(111) slabs shown in Fig. 1. Projector-augmented waves (PAW),[29–32] generalized gradient approximation (GGA),[33–35] as implemented in the Vienna *ab initio* simulation package (VASP),[36–38] were applied in the DFT calculations. In the plane wave calculations, a cutoff energy of 400 eV was applied, which was automatically set by the total energy convergence calculation for the Au(111), AuAg(111), and Ag(111) systems. For modeling the Au(111) surface, we adopted slabs containing three layers with four atoms per layer (Fig. 1a). The surface was constructed as a slab within the three dimensional periodic boundary condition, and models were separated from their images in the direction perpendicular to the surface by a 14 Å vacuum layer. In Au(111) model, the supercell dimension was 5.767 × 5.767 × 18.709 Å^3. In Ag(111) model, the supercell dimension was 5.778 × 5.778 × 18.717 Å^3. For these calculations, a 7 × 7 × 1 *k*-point mesh was used in the 2 × 2 super cell. The bottom layer was kept fixed to the bulk coordinates; full atomic relaxations were allowed for the top two layers. The atoms in the cell were allowed to relax until the forces on unconstrained atoms are less than 0.01 eV Å^{-1}. The contour map of Fig. 1d–f correspond to slide models of Au(111) and AuAg(111) and Ag(111).

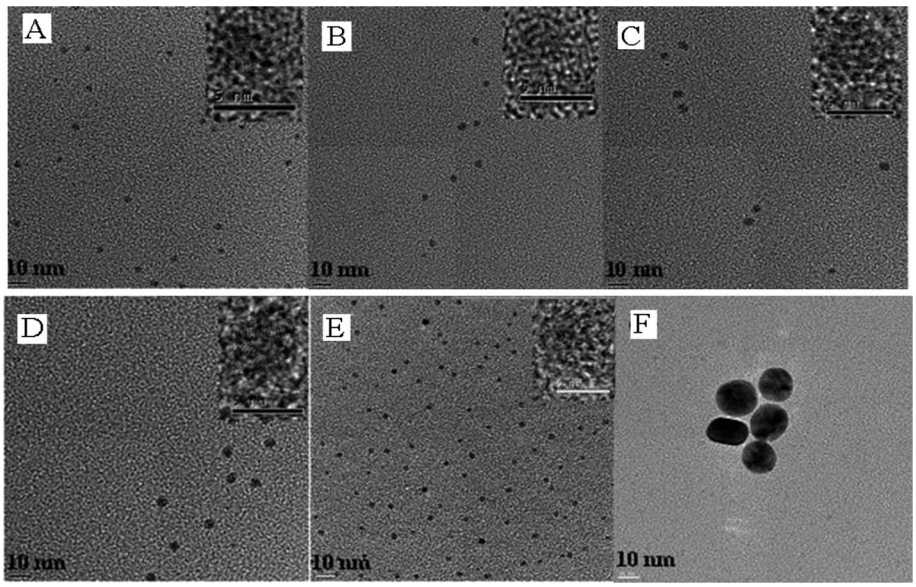

Fig. 2 Representative TEM images of the Au_xAg_{10-x} NPs (A) Ag, (B) Au_1Ag_9, (C) Au_5Ag_5, (D) Au_7Ag_3, (E) Au_9Ag_1 and (F) Au. Insets show the corresponding HRTEM images.

Results and discussion

Fig. 2 presents typical transmission electron microscopic (TEM) images of the Au_xAg_{10-x} NPs. The subscripts in Au_xAg_{10-x} indicate the apparent ratio, which is defined by the amount of Au and Ag salts added to the reaction mixture during the synthesis. The corresponding high-resolution TEM (HRTEM) images of these NPs are shown as insets. The Au_xAg_{10-x} NPs were well dispersed with particle sizes around 3–5 nm. An exception was for the pure Au NPs. In this case, the synthesis yielded NPs with mean particle size of about 20–25 nm, with a relative narrow size distribution. Several attempts to prepare Au NPs with diameters in the 3–5 nm range using the PVP method were unsuccessful. In any case, the SERS investigations were carried out for the Au NPs and the results compared with the alloy NPs. We would like to argue that this size difference will not significantly affect the trend of the SERS effect on the composition, because the NPs were heavily aggregated (dried on glass slides using a hot plate), which minimized the size effect. Although, this difference in size should be noted, the presence of the pure gold data point in the SERS intensity trend plots is not essential to support the main conclusions of this work.

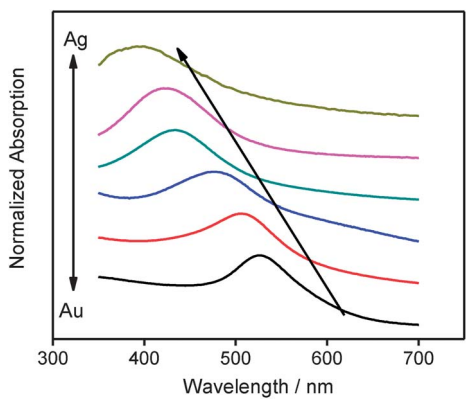

Fig. 3 UV-Vis extinction spectra of the Au_xAg_{10-x} NPs. From top to bottom: Ag, Au_1Ag_9, Au_5Ag_5, Au_7Ag_3, Au_9Ag_1, and Au. The spectra were taken after diluting the NPs in methanol.

The composition of the bimetallic NPs can be monitored through UV-Vis extinction measurements, as shown in Fig. 3. Two important aspects of Fig. 3 are: (1) the maximum in extinction shifts linearly with the NPs composition from ~400 nm (pure Ag) to ~530 nm (pure Au). The extinction maximum is related to the excitation of localized surface plasmons (LSPs) from these structures, and the resonance wavelength is expected to increase with the gold ratio. The linear SP-energy shift with the composition has been assigned to a homogeneous distribution of metals within the alloy;[16] (2) there were no clear contribution (which should manifest as additional extinction peaks) from the pure metals in any of the UV-Vis of the alloys,[20] suggesting that just one type of NPs were present in the suspensions. Although the particle size also affects the position of the LSPR, this effect is less dramatic than the composition of the alloys.[39]

Four different probe molecules were used (their structures are presented in Fig. S2†) to evaluate the SERS characteristics of the NPs deposited on glass. The probe molecules were selected considering their chemical characteristics. Two thiols (HTP and TP) with similar structure (the only difference between then is an extra hydroxyl group in HTP) and two cation dyes (Oxa and NBA) were used. HTP and TP can be considered as Lewis bases that bind to the metal through their thiolate groups. On the other hand, Oxa and NBA are positively charged heterocyclic aromatic amines, and are expected to interact with the metal surface as Lewis acids. The objective of using two groups of chemicals with similar structures was to highlight the effect of

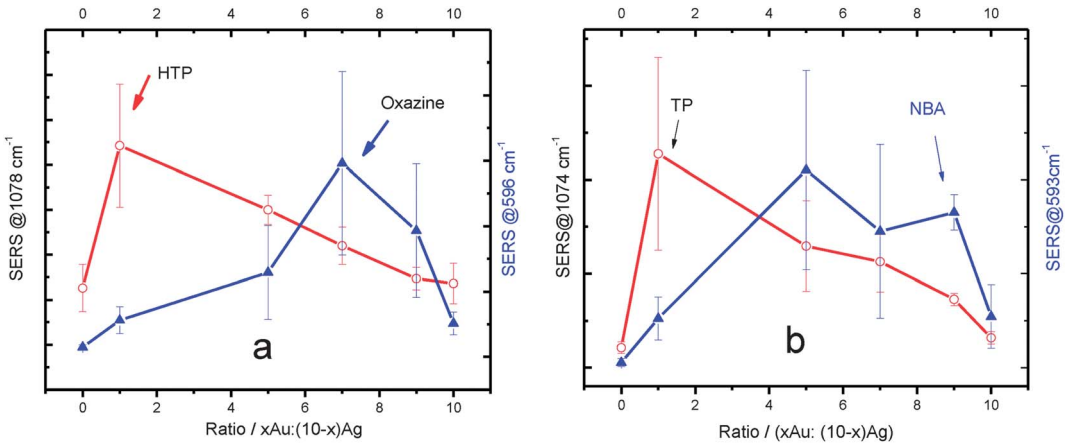

Fig. 4 Dependence of the SERS signal on the Au:Ag ratio. (a) HTP and Oxa; (b) TP and NBA. The error bars are the results of 5 measurements. 632.8 nm excitation.

the binding site on the SERS trend with the NPs composition. The use of two species of the same family (*e.g.*, two thiols) provided some redundancy that can be used to confirm the reliability of the experimental trends. Another important aspect is that the main electronic transitions for both HTP and TP are in the UV range, while Oxa and NBA absorbs in the red (around 600 nm). Therefore, an additional resonance Raman contribution is expected for Oxa and NBA under 632.8 nm excitation. The resonance Raman effect should increase the SERS efficiency for these dyes for red excitation, but should not affect the dependence of the scattering on the composition of the NPs.

Fig. 4 shows the variation of SERS intensities with the composition of the Au:Ag alloys obtained under 632.8 nm excitation. The scattering from the molecules adsorbed on the pure metal NPs were also plotted for comparison. The SERS intensities in Fig. 4 correspond to the height of the strongest band in the spectrum of each species. The ring breathing modes were used for both HTP ($\sim$1078 cm^{-1}) and TP ($\sim$1074 cm^{-1}) and phenoxazine ring stretching vibrations were used for Oxa ($\sim$596 cm^{-1}) and NBA ($\sim$593 cm^{-1}). The full spectrum from each species is available in Fig. S3.†

Fig. 4a shows that the SERS intensity from HTP at Au_1Ag_9 is larger ($\sim$4 times) than from HTP at pure Ag NPs. This shows that a relative small amount of gold (10% in the alloy) has a dramatic effect on the SERS intensity, in that particular case. After Au_1Ag_9, the SERS signal of HTP decreases as the Au:Ag ratio increases. Finally, the HTP SERS signal from pure Au NPs is similar in magnitude than from pure Ag NPs. The observed result agrees well with the trends that have been published in the literature.[12,19] A small amount of Au in Au:Ag alloys has been shown to enhance the SERS performance, but the SERS response deteriorates as the amount of Au increases in the alloy.

However, this trend is not followed by Oxa (Fig. 4a). Similarly to the HTP case, the addition of 10% gold into the alloy (Au_1Ag_9) results in an increase of the Oxa SERRS signal. However, in contrast to HTP, further increase in the amount of Au in the alloy composition leads to an increase in the SERRS signal, until a maximum is reached at Au_7Ag_3 (although it is important to point out that the SERRS intensities are quite close for Au:Ag ratios equals to 5 : 5, 7 : 3, and 9 : 1). It is then clear from Fig. 4a that: (1) in agreement to previous reports on both core–shell and alloy bimetallic NPs systems, the combination of the two metals leads to a better SERS performance, when compared to the pure metallic NPs;[12–14,19] (2) the two SERS probes tested demonstrated distinct enhancement trends with the composition of the NPs, which is a very interesting effect that has not been reported before.

The adsorption of ionic species to charged metallic surfaces can be accomplished through ion-pair interactions. A control experiment was performed to demonstrate that this effect does not significantly alter the observed trend. In the control experiment, the NPs were mixed with excess KCl (equal volumes of NP suspension, containing Oxa, and 0.1 M KCl solution) before drying. The NPs dried in the excess of KCl presented a slightly better SERRS efficiency (see Fig. S5†), but the only spectral difference was the presence of a strong metal–halide stretching in the low frequency range. In terms of SERRS intensity trend with the NPs composition, the presence of excess KCl shifted the position of the maximum SERRS to the 9Au : 1Ag in the case of OXA (relative to 7Au : 3Ag, as shown in Fig. 4). This indicated that even the presence of excess halides might affect the composition of optimal SERRS performance, although the qualitative trend for this species (best SERRS enhancement factor at higher gold compositions) remained the same.

In order to further confirm the results from Fig. 4a, the experiments were repeated with two different probe molecules, TP and NBA. The TP and NBA binding to the metal surfaces should be equivalent to HTP and Oxa, respectively, since they have very similar structures. The use of different molecules with similar chemical characteristics increase the confidence that the trends are not related to contaminations or artifacts. The experimental results for both TP and NBA are shown in Fig. 4b. Not surprisingly, TP showed almost exactly the same trend as HTP. In the case of NBA, the optimum Au:Ag ratio did not exactly match the observed for Oxa. However, the overall trend was still the same: higher gold ratio led to better SERS signal. The results in Fig. 4 are very interesting because they show the effect of the chemical characteristics of the probe on the SERS efficiency of the substrate. This demonstrates that an "optimized substrate" for HTP and TP is achieved at different NPs

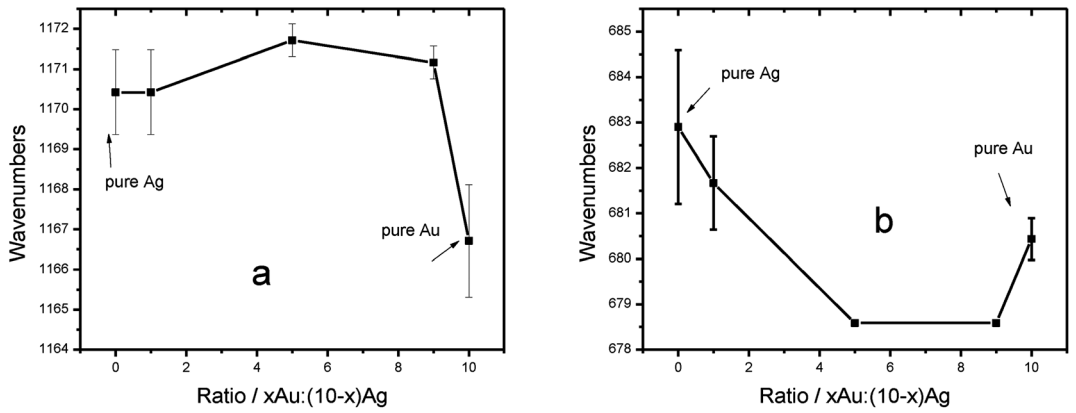

Fig. 5 Dependence of the SERS band position with the alloy composition (a) HTP and (b) Oxa. Error bar were calculated from 5 measurements.

composition than for Oxa and NBA. The effect of the molecular probe might then constitute another variable (together with excitation wavelength[6]) that need to be considered when comparing novel substrates reported in the literature.

Molecular effects in SERS are not new. In fact, there are a family of contributions to the surface-enhancement that take into consideration the electronic structure of both the adsorbed molecule and the metal–adsorbate complex. For instance, one of these "chemical" contributions to SERS involves the charge-transfer (CT) effect. In this case, the contribution to the overall enhancement is related to the resonant excitation of electrons from the metal's Fermi level to a molecular frontier orbital.[40] The resonance with the excitation is a common characteristic of the chemical contributions, including the CT effect. Therefore, a well-established approach to prove the role of chemical mechanisms is to explore the dependence of the SERS signal with the excitation wavelength. The argument in our particular case would be as following: the chemical contribution to the SERS effect will maximize at a particular alloy composition that enables a CT complex with the excitation, because the Fermi level in the alloy is tuned by the composition. If that is the case, the maximum SERS would occur at different compositions for different excitation wavelengths. Two laser frequencies (632.8 nm and 785 nm) were used to excite SERS of both HTP and Oxa, but no difference in the trend was found (spectra presented as Fig. S4†). These results suggest that the chemical-specific SERS trends with the alloy composition cannot be explained by a CT mechanism.

DFT calculations on pure Ag, pure Au, and Au:Ag alloys were performed to provide additional insights into the chemical-specific trends presented in Fig. 4. The DFT results are summarized in Fig. 1, and in the Table S1 and Fig. S1 of the ESI.† The DFT data for the 1 : 1 Au:Ag alloy (AuAg (111)) shows a charge donation from Ag to Au (0.164 e transferred from Ag to Au). As a result, the silver atoms in the alloys are partially positively charged, while the gold atoms are partially negatively charged, in agreement to previous reports.[30–32] The silver domains in the alloy surface can be treated as a weak Lewis acid, while the gold domains can be treated as weak Lewis base. Considering the chemical structures of the SERS probes, it is reasonable to expect that HTP and TP will preferentially bind to the silver rich domains in the alloys, while Oxa and NBA will likely bind to gold domains. This type of selective binding has been observed for the case of pyridine that preferentially interacts with silver in Au:Ag alloys.[30]

The selective interaction of the adsorbate with a component of the alloys can be validated by analyzing the position of their vibrational bands. The vibrational frequency depends on the nature of the binding between the molecule and the metal and small (but significant) shifts might be evident.[18,20,26,27,41] The position of the vibrational band of the adsorbate has actually been previously used to identify the surface composition of alloy NPs.[26,27,42]

Fig. 5 shows the dependence of the SERS peak position of the ring breathing and the ring stretching modes of HTP and Oxa, respectively, on the composition of the alloys. Fig. 5a shows $\sim$4 cm^{-1} difference for HTP bounded to pure Ag compared to pure Au. The magnitude of the shift is in agreement to the observed from other groups.[18,26,27,42] The main aspect of Fig. 5a, however, is that the band position of HTP adsorbed on the alloy NPs of different composition are closer to the value from pure Ag. This holds true even when the alloy composition heavily favors the Au over the Ag. Fig. 5a strongly suggests then that the HTP molecules preferentially adsorb on Ag-rich domains in the alloy.[30] On the other hand, for the case of Oxa, presented in Fig. 5b, a different trend in the position of the SERS band with the alloy composition was observed. A 3 cm^{-1} difference between the pure silver and the pure gold is evident in Fig. 3b. The positions of the bands for Oxa adsorbed on the alloys that yielded the largest SERS (see Fig. 3a) are closer to the frequency of Oxa adsorbed on pure gold. Fig. 5 offers direct proof of selectively binding and clearly shows that the maximum SERS correlates to the binding to alloys with the largest compositions of the preferential binding sites (maximum SERS for HTP was for the alloy with the largest amount of Ag and the maximum SERS of Oxa was for the alloy with the largest amount of Au). Wu *et al.*[42] calculated the Raman spectra of pyridine adsorbed on Ag and Au clusters and found a frequency dependence with the cluster type. Our results corroborate that work experimentally and contribute an additional dependence of the shift with the

alloy composition, which should be connected to the degree of charge donation among the atoms in the alloy.

The selective adsorption revealed by Fig. 5 suggests that the maximum SERS enhancement should be related to the metal–molecule interaction at the preferential sites. Using the HTP case as an example, a small amount of Au (about 10%) in the alloy leads to a charge separation that will favor its adsorption to the silver domains. This preferential adsorption should increase the surface concentration of HTP leading to an increase (~4 times) in SERS intensity. Notice that in a simple Langmuir adsorption model (below surface coverage saturation), this increase in surface concentration would require a 4-fold increase in the equilibrium adsorption constant. This is very feasible, since this would require only a modest decrease in the free energy of adsorption, due to its exponential relationship with the adsorption constant.

Conclusion

Au:Ag bimetallic alloys NPs were prepared using EG and PVP. The alloy NPs were characterized by HRTEM, and UV-Vis extinction spectroscopy. The SERS properties from two classes of probes at two different excitation laser frequencies were evaluated. Maximum SERS was observed for the alloys in all probes; however, the composition of the alloy that enabled the maximum was dependent on the chemical nature of the probe molecules. This clearly indicates that the probe molecule must be taken into account on SERS substrates optimization. DFT calculations confirmed a charge donation from Ag to Au atoms in the alloys. This charge donation promotes selective binding of probe molecules to different metallic domains on the bimetallic alloy surface. This preferential binding has a direct influence in the SERS characteristics of the adsorbed molecule in the alloy surface.

Acknowledgements

This work was supported by NSERC through the discovery grant program and through the Strategic Network for Bioplasmonic Systems (Biopsys). M.F. thanks the Natural Science Foundation of China (grant no. 21105092) for financial support.

References

1 M. G. Albrecht and J. A. Creighton, *J. Am. Chem. Soc.*, 1977, **99**, 5215–5217.
2 J. N. Anker, W. P. Hall, O. Lyandres, N. C. Shah, J. Zhao and R. P. Van Duyne, *Nat. Mater.*, 2008, **7**, 442–453.
3 J. F. Li, Y. F. Huang, Y. Ding, Z. L. Yang, S. B. Li, X. S. Zhou, F. R. Fan, W. Zhang, Z. Y. Zhou, D. Y. Wu, B. Ren, Z. L. Wang and Z. Q. Tian, *Nature*, 2010, **464**, 392–395.
4 X. M. Qian, X. H. Peng, D. O. Ansari, Q. Yin-Goen, G. Z. Chen, D. M. Shin, L. Yang, A. N. Young, M. D. Wang and S. M. Nie, *Nat. Biotechnol.*, 2008, **26**, 83–90.
5 M. K. Fan, G. F. S. Andrade and A. G. Brolo, *Anal. Chim. Acta*, 2011, **693**, 7–25.
6 I. A. Larmour, K. Faulds and D. Graham, *Chem. Sci.*, 2010, **1**, 151–160.
7 M. E. Stewart, C. R. Anderton, L. B. Thompson, J. Maria, S. K. Gray, J. A. Rogers and R. G. Nuzzo, *Chem. Rev.*, 2008, **108**, 494–521.
8 C. J. Addison and A. G. Brolo, *Langmuir*, 2006, **22**, 8696–8702.
9 M. Fan and A. G. Brolo, *Phys. Chem. Chem. Phys.*, 2009, **11**, 7381–7389.
10 J. R. Anema, A. G. Brolo, P. Marthandam and R. Gordon, *J. Phys. Chem. C*, 2008, **112**, 17051–17055.
11 Q. Min, M. J. L. Santos, E. M. Girotto, A. G. Brolo and R. Gordon, *J. Phys. Chem. C*, 2008, **112**, 15098–15101.
12 Y. Cui, B. Ren, J. L. Yao, R. A. Gu and Z. Q. Tian, *J. Phys. Chem. B*, 2006, **110**, 4002–4006.
13 N. R. Jana, *Analyst*, 2003, **128**, 954–956.
14 G. V. P. Kumar, S. Shruthi, B. Vibha, B. A. A. Reddy, T. K. Kundu and C. Narayana, *J. Phys. Chem. C*, 2007, **111**, 4388–4392.
15 A. G. Shen, L. F. Chen, W. Xie, J. C. Hu, A. Zeng, R. Richards and J. M. Hu, *Adv. Funct. Mater.*, 2010, **20**, 969–975.
16 R. Ferrando, J. Jellinek and R. L. Johnston, *Chem. Rev.*, 2008, **108**, 845–910.
17 R. A. Alvarez-Puebla, D. J. Ross, G. A. Nazri and R. F. Aroca, *Langmuir*, 2005, **21**, 10504–10508.
18 L. Y. Cao, P. Diao, L. M. Tong, T. Zhu and Z. F. Liu, *ChemPhysChem*, 2005, **6**, 913–918.
19 Y. Cui and R. A. Gu, *Chem. Res. Chin. Univ.*, 2005, **26**, 2090–2092.
20 R. G. Freeman, M. B. Hommer, K. C. Grabar, M. A. Jackson and M. J. Natan, *J. Phys. Chem.*, 1996, **100**, 718–724.
21 L. Ling, M. M. Xu, R. A. Gu and J. L. Yao, *Acta Chim. Sin.*, 2007, **65**, 779–784.
22 Y. C. Liu, K. H. Yang and S. J. Yang, *Anal. Chim. Acta*, 2006, **572**, 290–294.
23 L. H. Qian, Y. Ding, T. Fujita and M. W. Chen, *Langmuir*, 2008, **24**, 4426–4429.
24 L. Rivas, S. Sanchez-Cortes, J. V. Garcia-Ramos and G. Morcillo, *Langmuir*, 2000, **16**, 9722–9728.
25 M. Wang, J. L. Yao and R. A. Gu, *Chem. Res. Chin. Univ.*, 2006, **27**, 1518–1521.
26 K. Kim, K. L. Kim, J. Y. Choi, H. B. Lee and K. S. Shin, *J. Phys. Chem. C*, 2010, **114**, 3448–3453.
27 K. Kim, K. L. Kim and S. J. Lee, *Chem. Phys. Lett.*, 2005, **403**, 77–82.
28 E. Hao, S. Y. Li, R. C. Bailey, S. L. Zou, G. C. Schatz and J. T. Hupp, *J. Phys. Chem. B*, 2004, **108**, 1224–1229.
29 D. Vanderbilt, *Phys. Rev. B: Condens. Matter Mater. Phys.*, 1990, **41**, 7892–7895.
30 P. E. Blochl, *Phys. Rev. B: Condens. Matter Mater. Phys.*, 1994, **50**, 17953–17979.
31 M. C. Payne, M. P. Teter, D. C. Allan, T. A. Arias and J. D. Joannopoulos, *Rev. Mod. Phys.*, 1992, **64**, 1045–1097.
32 G. Kresse and D. Joubert, *Phys. Rev. B: Condens. Matter Mater. Phys.*, 1999, **59**, 1758–1775.

33 P. Hu, D. A. King, S. Crampin, M. H. Lee and M. C. Payne, *Chem. Phys. Lett.*, 1994, **230**, 501–506.
34 J. P. Perdew, J. A. Chevary, S. H. Vosko, K. A. Jackson, M. R. Pederson, D. J. Singh and C. Fiolhais, *Phys. Rev. B: Condens. Matter Mater. Phys.*, 1992, **46**, 6671–6687.
35 H. Eschrig and P. Ziesche, European Physical Society and Technische Universität Dresden. Institut für Theoretische Physik, *Electronic structure of solids '91*, Akademie Verlag, Berlin, 1991.
36 G. Kresse and J. Hafner, *Phys. Rev. B: Condens. Matter Mater. Phys.*, 1993, **47**, 558–561.
37 G. Kresse and J. Furthmuller, *Phys. Rev. B: Condens. Matter Mater. Phys.*, 1996, **54**, 11169–11186.
38 G. Kresse and J. Furthmuller, *Comput. Mater. Sci.*, 1996, **6**, 15–50.
39 J. Zhu, *Phys. E*, 2005, **27**, 296–301.
40 A. G. Brolo, D. E. Irish and B. D. Smith, *J. Mol. Struct.*, 1997, **405**, 29–44.
41 G. F. S. Andrade, A. G. Brolo and M. L. A. Temperini, *J. Phys. Chem. C*, 2008, **112**, 15348–15355.
42 D. Y. Wu, B. Ren and Z. Q. Tian, *ChemPhysChem*, 2006, **7**, 619–628.